Bioinspiration & Biomimetics

PAPER

Detachment of the remora suckerfish disc: kinematics and a bio-inspired robotic model

To cite this article: Siqi Wang *et al* 2020 *Bioinspir. Biomim.* **15** 056018

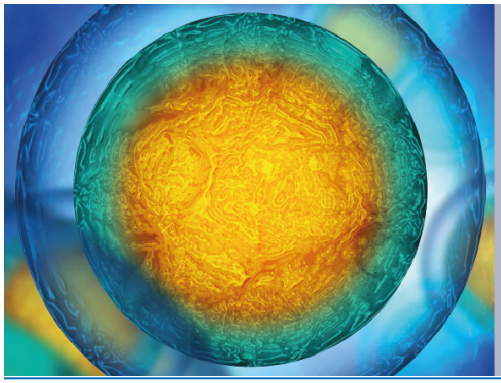

Bioinspiration & Biomimetics

PAPER

Detachment of the remora suckerfish disc: kinematics and a bio-inspired robotic model

RECEIVED
30 January 2020

REVISED
26 March 2020

ACCEPTED FOR PUBLICATION
18 May 2020

PUBLISHED
21 August 2020

Siqi Wang[1,5,6], Lei Li[1,6], Wenguang Sun[1,6], Dylan Wainwright[2], He Wang[1], Wei Zhao[1], Bohan Chen[1], Yufeng Chen[3,4] and Li Wen[1,7]

[1] School of Mechanical Engineering and Automation, Beihang University, Beijing, 100191, People's Republic of China
[2] The Museum of Comparative Zoology, Harvard University, Cambridge, MA 02138, United States of America
[3] Department of Electrical Engineering and Computer Science, Massachusetts Institute of Technology, Cambridge, MA 02139, United States of America
[4] John A. Paulson School of Engineering and Applied Sciences, Harvard University, Cambridge, MA 02138, United States of America
[5] Shenyuan Honors College, Beihang University, Beijing, 100191, People's Republic of China
[6] These authors contributed equally to this paper.
[7] Author to whom any correspondence should be addressed.

E-mail: liwen@buaa.edu.cn

Keywords: bio-inspired robotics, underwater adhesion, remora suckerfish

Supplementary material for this article is available online

Abstract

Remora suckerfish can attach to a wide diversity of marine hosts, however, their detachment mechanism remains poorly understood. Through analyzing high-speed videos, we found that the detachment of the live remora (*Echeneis naucrates*) is a rapid behavior that can happen within 240 ms. We separate this remarkable behavior into three stages: 1) lamellae folding down and soft lip curling, 2) disc raising and 3) complete detachment. To quantitatively investigate the detachment behavior, we fabricated a multi-material biomimetic disc and utilized it to study each stage of the detachment process. In stage one, we found that folding down lamellae is essential for decreasing the detachment resistance (vertical interfacial force and friction force) of the suction disc. Also, curling up the soft lip to breaking the adhesive seal reduced the vertical pull-off force up to 94 times. During disc raising in stage 2, we found that the partially flexible base (Young's modulus: ∼3 MPa) of the disc can lead to a 30% power-use reduction compared to a rigid base (Young's modulus: ∼3 GPa). After completing full detachment in stage 3, the corresponding drag wake flow decreased by 44% compared to an attached state due to lamellae folding and the entire soft lip uncurling. We developed a bio-inspired remora suckerfish robot propelled by a water jet to demonstrate a complete detachment which covers all three stages within 200 ms. We also demonstrated that an ROV has both hitchhiking and pick-and-place capabilities by integrating remora-inspired discs at appropriate locations. This study may shed light on future research in bio-inspired adhesives and lay a foundation for developing an untethered, multimodal, underwater hitchhiking robot.

1. Introduction

Animals in nature have evolved various adhesive organs (see figure 1(a)) to achieve diverse behaviors, including climbing, perching, feeding and evading predators [1, 2]. However, once adhered to a surface, rapid detachment often becomes a necessary skill, lest an organism provides an easy meal for a predator. Across a range of sizes, diverse attachment and detachment mechanisms of animals have adapted to both dry and wet natural environments (figure 1). In the terrestrial environment, insects including ants [3], beetles [4], flies [5], and cockroaches [6] (with a mass ranging from $\sim 10^{-4}$ to ∼10 g) utilize smooth, hairy, or clawed pads to interlock with natural substrates and generate strong adhesive forces, while mechanically un-locking or peeling the pads enables detachment. Among vertebrates, geckos are well-know users of dry adhesion [7]. These lizards adhere using hierarchical structures on their feet that generate intermolecular forces and they detach by hyperextending their toes to peel off their feet. Tree frogs are capable of attaching to wet surfaces using pads with microscale channels and they detach by tuning

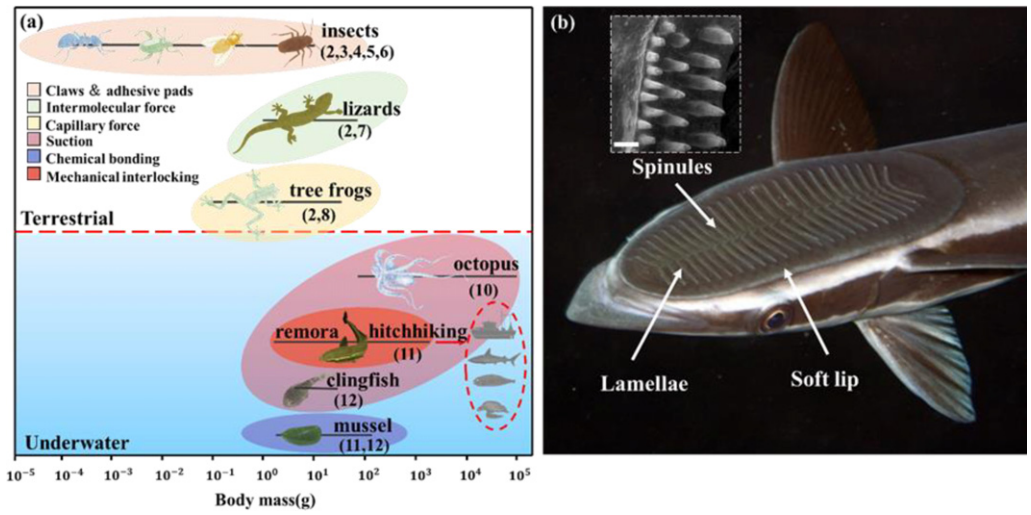

Figure 1. Various adhesion mechanisms of animals with different body mass. (a) In the terrestrial environment, insects interlock with substrates using claws and adhesive pads. Geckos and tree frogs employ the intermolecular forces and capillary forces to achieve climbing. In the underwater environment, octopus and clingfish attach to objects through the pressure differential generated by suction adhesion, while mussels use proteinaceous chemical bonding. In remoras the hierarchical disc structure enables the regulation of the adhesion force, allowing it to attach to various moving hosts. (b) Soft lip, lamellae and spinules of a biological remora suction disc. (Photo credit: Klaus M. Stiefel). Inset: Environment scanning electron microscope (ESEM) image of biological spinules. Scale bar, 200 μm.

both limb and toe angles from high adhesion to low adhesion states [8]. Wet adhesion in an immersed underwater environment requires different strategies than above because mechanisms such as van der Waals and capillary forces are ineffective [9]. Marine organisms mainly utilize two types of adhesion in submerged environments: chemical adhesion and suction adhesion. By secreting chemical adhesives, such as the proteins DOPA and hydroxyproline, mussels can permanently attach themselves to rocks and surfaces to withstand ocean waves [10, 11]; however, mussels have no capacity for self-detachment. Cephalopods [12] and some fishes use biological suction cups to achieve reversible attachment on various substrates. In particular, clingfishes achieve underwater attachment using a ventral adhesive disc covered with papillae and they detach by controlling the pectoral fin as a 'valve' for releasing the seal [13–15].

The remora suckerfish (*Echeneis naucrates*) has a highly-modified suction disc on the dorsal side of its head and is capable of fast and reversible adhesion to fast-moving marine hosts, including sharks, other fishes, turtles and boats [16, 17]. According to previous studies [18, 19], a remora's suction disc consists of three main functional components (see figure 1(b)): a lip surrounding the disc that forms the seal at the hosts' surface; many paired rows of bony lamellae in the center of the disc that can erect and fold to tune the disc's pressure differential; and microscale bony spinules protruding from the lamellae, which help enhance frictional force. Hitchhiking behavior requires a remora to be capable of both attaching and detaching regularly and while a number of studies have focused on remora attachment [20–22] and corresponding biomimetic prototypes [23, 24], the detachment of remoras is poorly understood. Understanding detachment is essential in studying biological adhesive systems and is becoming increasingly important in many engineering applications such as surface peeling (surface painting, coating and transfer printing, etc) [25–27]. Thus, exploring how a remora can detach (i.e. a 'self-peeling' process) would expand the horizons of understanding the biological system and may further inspire future artificial adhesion mechanisms. We focus our research here on two central questions: 1) How do disc components (i.e., the disc pad, disc lip and the lamellae with spinules) synergistically move to enable detachment of a live remora? 2) How does each component affect the force, power, and speed of a remora's detachment?

In our previous study, we developed a biomimetic remora disc that can attach to several substrates with different roughness by carefully mimicking the morphology and kinematics of a remora's suction disc, but this past platform detaches by pumping water into the disc to eliminate chamber pressure differential [28]. Although we previously implemented a simplified engineering approach to detachment by curling the anterior disc lip to equalize the internal and external pressure [29], the synergistic motion between the disc pad, disc lip and lamellae with spinules remains unexplored. In the current study, we systematically explored the detachment kinematics and associated morphology of live remoras (*Echeneis naucrates*). We then developed a biomimetic flexible adhesive disc with controllable motion of both the disc lip and the lamellae with spinules. We systematically quantified the contributions of lamellae motion, disc flexibility, the soft lip motion on adhesive and detachment performance. Furthermore, we designed a remora robot

that can demonstrate complete detachment behavior and we also mounted the biomimetic remora disc to an ROV to demonstrate simple applications.

2. Materials and methods

2.1. Observation of live remoras' detachment

Three live remoras (body length: 25 ± 5 cm) were collected from licensed fishermen in the South China Sea. We kept remoras in a laboratory aquarium with a dimension of 60 × 30 × 33 cm at a temperature of 24 °C. The remoras used in this study follow the regulations for the Administration of Affairs Concerning Experimental Animals issued by the Institutional Animal Care and Use Committee of Beijing.

To investigate the kinematics of remoras' detachment, we used a food stimulus (the shrimp *Exopalaemon carinicauda*) to elicit detachment. After placing food above the remoras, they detached from the bottom of the tank (60 × 30 × 33 cm) and swam to eat the prey. Two synchronous high-speed cameras (FASTCAM Mini UX100, Photron Ltd, Tokyo, Japan) filming at 500 frames-per-second recorded the detachment processes from tank lateral and bottom views (the dorsal suction cup of the remora suckerfish adhered to the bottom of tank). At least ten detachment videos were filmed for each remora for a total of over 30 high-speed detachment videos of live remoras. The kinematic analysis (disc rising angle α and the angular velocity ω, figure 2) were performed in the motion tracking software PROANALYST (Xcitex Inc, Woburn, USA).

To study the morphology used in detachment, we generated a μCT (micro computed tomography) scan of a remora head that had been stained for two weeks with 2% phosphomolybdic acid (PMA) in a solution of 70% ethanol. The PMA stained soft tissues and allowed for us to examine the anatomy of the soft disc lip and any associated muscles (otherwise μCT is limited to mineralized tissues). The remora head was loaned from the Museum of Comparative Zoology at Harvard University (MCZ Ichthyology #83209) and was scanned with a Skyscan 1173 benchtop system (Bruker microCT, Kontich, Belgium) using a pixel size of 35.09 μm, 80 kV and 100 μA. Morphology of remora bones and muscles was reconstructed using Mimics v20 (Materialise, Leuven, Belgium).

2.2. Design and fabrication of the biomimetic remora disc

Following the procedures in our previous study, we designed and fabricated a multi-material biomimetic remora disc with attachment ability based on live-remora features [25]. The bio-robotic remora disc consists of three distinct features: the soft fleshy lip around the disc edge, rows of lamellae along the disc length and the bony spinules on each lamella. To achieve the detachment of the bio-inspired robot in the current study, we designed and fabricated a flexible cable-driven detachment mechanism for the remora-inspired adhesive disc (figure 3(b)). The detachment mechanism consists of three main parts: curling components, a 3D-printed slider mechanism and a miniature hydraulic cylinder (CJPB6-10, SMC Corp., Tokyo, Japan). Fabricated by a multi-material 3D printer Objet Connex C3 (Stratasys Ltd, Eden Prairie, MN, USA), each curling component consists of a series of rigid skeletons (VeroWhitePlus RGD835) and soft cladding material (TangoPlus FLX930) as the connections. The rigid skeletons can provide a greater curling force, while the soft cladding material was glued to the backside of the soft lip (inset panel of figure 3(b)). Three Kevlar ropes (0.8 mm in diameter) that connect with the slider pass through the holes of the three curling components. The hydraulic miniature cylinder was fixed on one support and actuated the slider's movement. When the miniature hydraulic cylinder is pressurized, the cables pull back through the slider mechanism. Different from the previous disc that has a rigid disc base, we designed and 3D printed the middle portion of the current disc base using soft materials (FLX9970-DM). This feature makes the disc base flexible and allows it to bend. The lamellae can erect to the specified angle controlled by the soft hydraulic actuators. The entire disc prototype was 127 mm long and 72 mm wide, with a total mass of 150 g.

2.3. Experimental procedure of the detachment process of the biomimetic remora disc

We conducted a series of experiments to investigate the detachment performance (curling force, pull-off force, forward frictional force, disc-raising force and resistance force) of the biomimetic remora disc. These results explain how each stage of the detachment mechanism contribute to remora detachment.

To explore stage 1 of the detachment process (soft lip curling and the lamellae raising), we experimentally measured the curling force, pull-off force and the inner pressure of the soft lip under different lamellae pitch angles (0°, 4°, 8°, 12° and 16°) using the experimental set-up shown in figure S1 (https://stacks.iop.org/BB/15/056018/mmedia). These experiments were conducted in a water tank with a size of 60 cm × 30 cm × 30 cm. The depth of the experimental substrate (smooth surface, $Ra = 0$ μm) was set as 20 cm; the prototype was fully immersed underwater and gently placed on the substrate before the experiment. A fixed pulley was installed directly above the anterior artificial curling muscle. A Kevlar rope was fixed to the top of the disc through the pulley, with another end connected to a robotic arm (MOTOMAN MH3F, YASKAWA Inc., Japan). We used a multi-axis force sensor (Mini 40 F/T sensor, ATI Technologies Inc., USA) to measure the force. To ensure the attachment of the biomimetic suction disc, an extra 20 N preload (equivalent to 2.3 KPa pressure) was applied to the prototype for 5 s

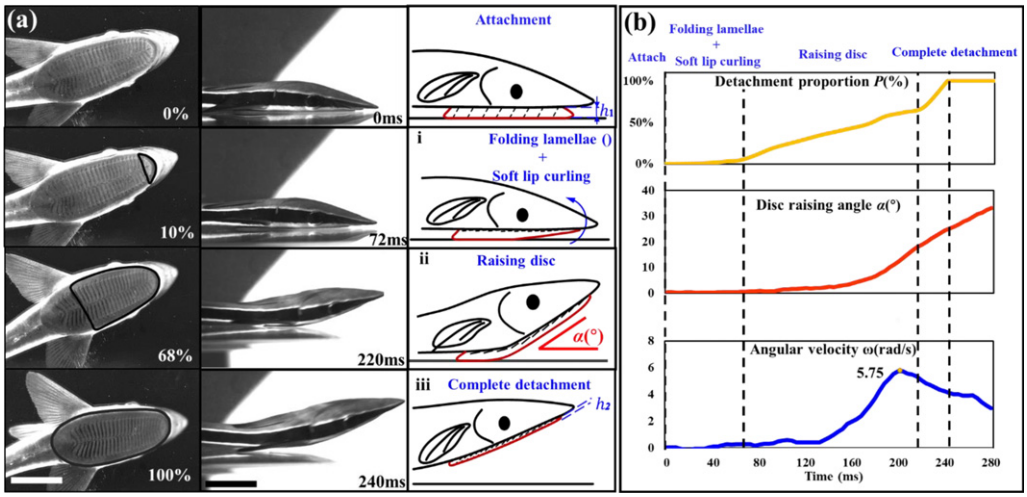

Figure 2. Kinematic mechanism of the remora's detachment. (a) High-speed images (tank bottom and side views; remora dorsal and lateral view) and corresponding schematics during a remora's detachment process including stage 1–3. In the bottom views, the disc in the black outline and the white numbers indicate the detached parts and the detached percentages, respectively. h_1 and h_2 represent the thickness of the suction disc before detachment and after detachment, respectively. Scale bar 2 cm. Panel (a) is reproduced with permission from IEEE (Wang *et al*, 2019). (b) Representative kinematic parameters over time during the detachment process. 5.75 rad s^{-1} is the maximum angular velocity of the remora during the disc raising stage

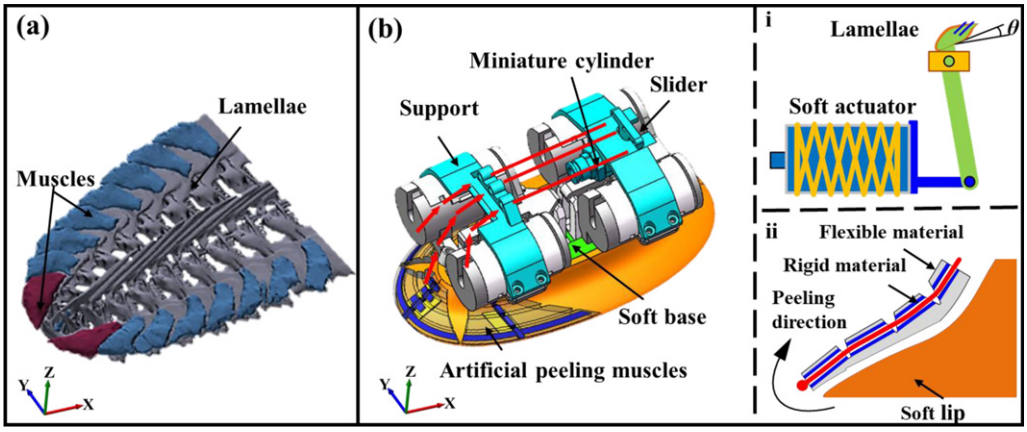

Figure 3. Design and fabrication of the disc prototype. (a) μCT image of the remora suction disc showing ventral view of the disc. Lip muscles are symmetrically distributed along the ventral side around the disc edge. Red-colored lip muscles contract first to curl the anterior-most portion of the soft lip, and blue-colored muscles contract after to continue curling the lip toward the disc posterior. (b) CAD model of the biomimetic remora disc with a detachment mechanism. The inset (i) shows that the lamellae motion is controlled by the soft actuator and θ refers to the lamellae pitch angle. The inset (ii) shows the cross-sectional schematic of the detachment mechanism. The internal channels (dark blue) and covering layer (translucent) were simultaneously printed with rigid and flexible materials, respectively. Panel (b) is reproduced with permission from IEEE (Wang *et al*, 2019).

at the beginning of each force experiment. The curling component curls up the anterior disc lip; then, the robotic arm moved upward at a speed of 40 mm s^{-1}. The force data were acquired by a data acquisition board (PCI 6284, National Instruments Corp., TX, USA) and LabVIEW 12.0 (National Instruments Corp., 2012) with a sampling rate of 50 Hz. A pressure sensor (ZSE30AF-01-N, SMC Corp., Tokyo, Japan) located at the center of the disc was used to measure the inner-chamber pressure when the lamellae pitch angle increased from 0° to 16° in steps of 2°.

To study stage 2 of detachment (the disc-raising stage), we explored the effect of disc-base flexibility on the force and energy of disc raising. We fabricated two prototypes, one disc with a soft base (FLX9970-DM, Young's modulus: ∼3 MPa), and another with a rigid base (VeroClear, Young's modulus: ∼3 GPa); the rest of the disc components remained the same. The soft material has a Young's modulus close to the same as the lip tissue (∼3 MPa vs ∼2.2 MPa, respectively), as measured in previous research [30]. The prototype was placed on the substrate in the experimental water tank, while the posterior end of the disc was fixed with acrylic plates and screws. A Kevlar rope linked the anterior part of the disc and the robotic arm. The robotic arm moved upward (the speed was set at 80 mm s^{-1}) until the Kevlar rope raised the

biomimetic disc to an angle of $\alpha = 30°$. This angle is similar to the disc-raising angle of the live remora. Through analysing high-speed videos of this event, we also measured the angular velocity (ω) of both disc prototypes under the same pulling force (10 N).

Compared with the attached state, the detached remora has a more flattened disc due to the soft lip and lamellae being adducted against the head. For stage 3 of detachment, we investigated the effect of the shape change of the disc on the overall fluid drag of the remora disc. To realize the shape change of the biomimetic disc, six artificial curling components were placed along the rim of the back of the soft lip and we used two servos to curl up the entire soft lip. We mounted the biomimetic disc in a circulating flow tank with a maximum speed of 0.5 m s^{-1} where the biomimetic disc was connected to the force sensor through a 25 cm long double-screw bolt. We immerse the biomimetic disc in the circulating tank and the distance between the water surface and the top surface of the biomimetic disc was 1 cm. Then we tested the fluid drag at the flow velocity of 0.5 m s^{-1}.

2.4. Statistic analysis

A commercial statistics software (Statistical Product and Service Solutions, IBM, New York, USA) was used for all statistical analysis. The values presented here are means ± standard deviation (s.d.). Our sample sizes were 15 for the kinematics of live remoras and 5 for bio-robotic experiments.

3. Results

3.1. Detachment of live remoras

Figure 2(a) shows high-speed video images and schematic views of a typical detachment response of a remora (*Echeneis naucrates*), and we separated the detachment mechanism into three stages. During stage 1, lamellae first rotate to move away from the substrate (0 ms) and the soft lip curls away from the surface from anterior to posterior to break the disc seal (72 ms). In stage 2, the remora raises its head away from the surface (ventral flexion in the remora frame-of-reference) with a maximum angular velocity of 5.75 rad s^{-1} to peel the adhesive disc away from the substrate immediately after the soft lip curls up (220 ms). In stage 3 the remora undulates its body and fins to pitch up the rest of the disc and swim away from the substrate (240 ms). After detachment, remoras flattened the entire disc against their head to swim freely.

The entire detachment process of the remoras took 315.5 ± 62 ms. Stage 1, 2 and 3 occupy 23 ± 6%, 60 ± 6%, and 17 ± 8% of the entire detachment time, respectively. We also measured the speed of the tip of the remora's head. The average vertical speed of detachment is 7.3 ± 0.83 cm s^{-1}. The maximum vertical speed of detachment is 28 ± 4.9 cm s^{-1} and happens in stage 3. The average forward speed of detachment is 7.4 ± 2.3 cm s^{-1}. The maximum forward speed is 29 ± 4.7 cm s^{-1} and happens in stage 3. More detailed kinematics variables versus time during the three stages are provided in figure 2(b) and a video of the process is available as supplementary movie S1.

During stage 1, the soft lip quickly curled away from the surface with an average angular speed of 34.3 ± 11.3 rad s^{-1}. Only the anterior disc lip (43 ± 4.9% of disc length) curled and a small part of the anterior of the suction disc (11 ± 3% of disc length) left the surface during stage 1 and anterior disc peeling averaged 72 ± 18.3 ms. During stage 1, the flexible disc base remains flat with a bending curvature k (3.2 ± 0.42) × 10^{-3} mm^{-1}, where k was calculated as 1/radius of disc curvature.

During stage 2, the anterior portion of the disc (68 ± 2% of disc length) detached from the substrate induced by the raising of the remora head away from the surface. Figure 2(b) shows the disc-raising angle α (defined as the angle between disc pad and the substrate) as a function of time t. The maximum angular velocity of the remora head (ω) during the detachment reaches up to 5.1 ± 0.75 rad s^{-1}. The posterior portion (32 ± 2%) of the disc (behind the neck position) remains in contact with the substrate. During stage 2, the flexible disc has a maximum bending curvature (κ) of (8.5 ± 0.9) × 10^{-2} mm^{-1}.

During stage 3, with the movements of the body and fins, the entire disc of the remora detaches from the surface with an averaged detachment angle $\alpha = 29$ ± 3°. At the same time, the remaining part (32 ± 2%) of the disc lip curls, thus achieving complete detachment. From the high-speed images (figure 2(a)), we found that the thickness of the adhesive disc after detachment (h_2 = 0.98 ± 0.12 mm) is significantly thinner than the attached state: h_1 = 1.97 ± 0.18 mm (ANOVA, $F = 153.405$; d.f. = 1; $P < 0.05$). The shape of the suction disc became flattened (κ is approximately 6.32 ± 0.82 × 10^{-3} mm^{-1}) due to the movements of lamellae and the soft lip after detachment.

3.2. The bio-robotic remora disc with detachment mechanism

To better understand the curling mechanism of the disc lip, we scanned a remora specimen using μCT (Bruker Skyscan, Kontich, Belgium). In figure 3(a), the scanning results show that lip muscles are distributed ventrally around the outer edge of the disc pad, with each muscle forming under a single lamella, except for the anterior-most pair of muscles. The ventral placement of these muscles puts them on the ventral side of the disc lip, which should cause them to curl the lip away from the surface when contracted. Contraction of the anterior-most lip muscles (rendered in red) will start to peel the disc and reduce the pressure differential (see movie S1). Based on this morphological feature and the lip-curling motion, we designed and fabricated artificial curling muscles (inset of figure 3(b)) and attached them to the same

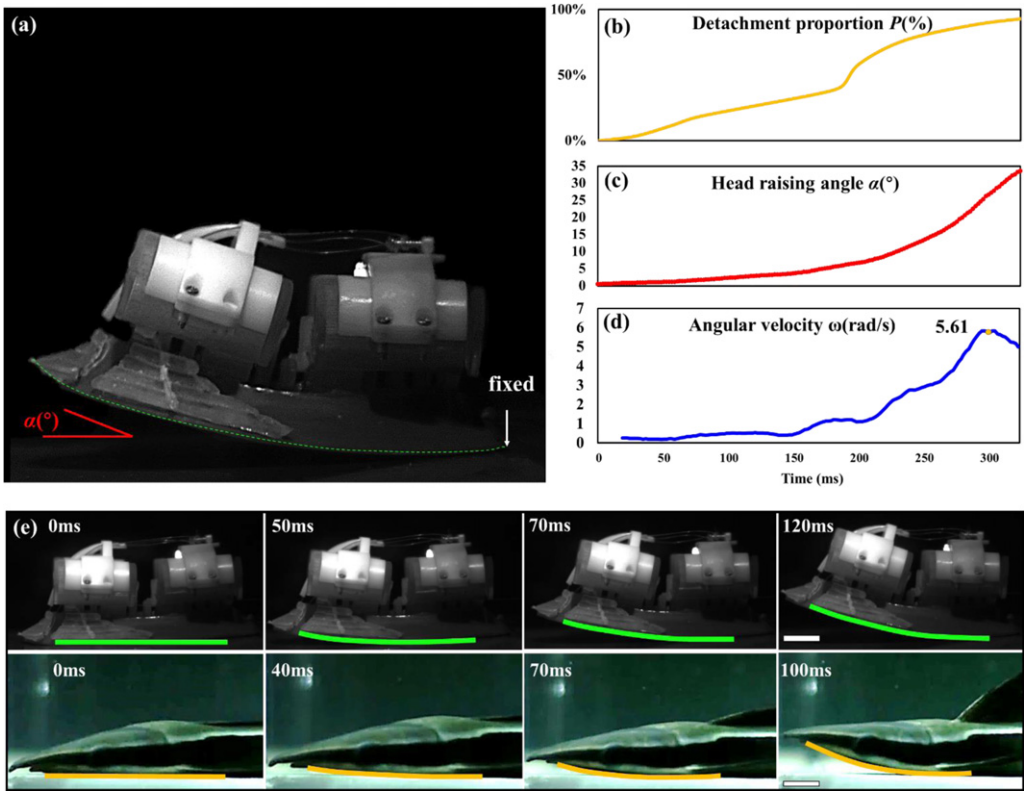

Figure 4. Kinematics of the biomimetic remora disc peeling motion during the disc-raising process. (a) We fixed the posterior end of the disc while raising the disc at the anterior end through a cable. The detachment proportion (P), the raising angle (α) and the angular velocity (ω) during the rising process are shown in panel (b)–(d). 5.61 is the maximum angular velocity during disc raising. (e) Comparison of detachment sequence between the biomimetic soft-base disc (scale bar 2 cm) and the remora disc (scale bar 1 cm). The contours (colored solid lines) of the disc lip show similar flexibility during disc raising.

positions seen in our μCT scan results (figure 3(b)). The motion sequence of three curling muscles can be programmed by adjusting the tension of the three Kevlar ropes. The miniaturized hydraulic cylinder actuates the three ropes to produce the curling of the soft lip (see supplementary movie S2).

Figure 4 shows that the bio-inspired disc prototype closely mimicked stage 2 of detachment based on an external load similar to the contraction of remora neck muscles (movie S3). Due to the soft base of the biomimetic disc, the contour shape (continuous lines) of the biomimetic disc demonstrates similar flexibility to the biological disc (figure 4(e) during the disc-raising process. figures 3(b)–(d) shows the kinematic data of the prototype during the head-raising, including the detachment proportion P, the head-raising angle α and the angular velocity ω. It is consistent with the kinematic data corresponding to the remora disc (figure 2(b)), which provides the basis for subsequent prototype experiments.

3.2.1. Detachment performance of stage 1

We found that that the motion of the lamellae has a notable effect on the soft lip's curling force, which triggers the detachment of the entire disc. Figure 5(a) shows the soft lip's curling force obtained from the experimental results as a function of the lamellae pitch angle. The curling force increased with the lamellae pitch angle. For example, the experimental curling force increased from 3.3 $\pm$ 0.30 N to 6.2 $\pm$ 0.22 N when the lamellae angle increased from 0° and 16°. During the attachment of the biomimetic disc, pressure differential (disparity between the inner chamber of the suction disc and external aquatic environment) as a function of the lamellae pitch angle is shown in figure 5(b). The pressure differential changed from -1.43 ± 0.07 to -12.21 ± 0.51 kPa when the lamellae pitch angle increases from 0° to 16°. Therefore, the curling force of the soft lip, in turn, depends on the pressure differential of the disc. We hypothesize that remora fold down the lamellae (decrease the lamellae angle) to reduce the peeling force needed at the anterior disc lip to start detachment.

We found that the force of dislodging the bio-robotic disc from the substrate increases with the lamellae angle. First, we show the force-time history of the bio-robotic disc during a peeling process while the disc has been unsealed by curling the soft lip (lamellae angle $\theta = 8°$, inset panel of figure 5(c)). The maximum force (F_{max}) is defined as the maximum instantaneous force during the detachment. The residual force (F_{re}) primarily includes the weight of the prototype, the buoyancy and the water resistance encountered by the prototype during the upward movement. The interfacial force (ΔF) is defined as the difference between F_{max} and F_{re}.

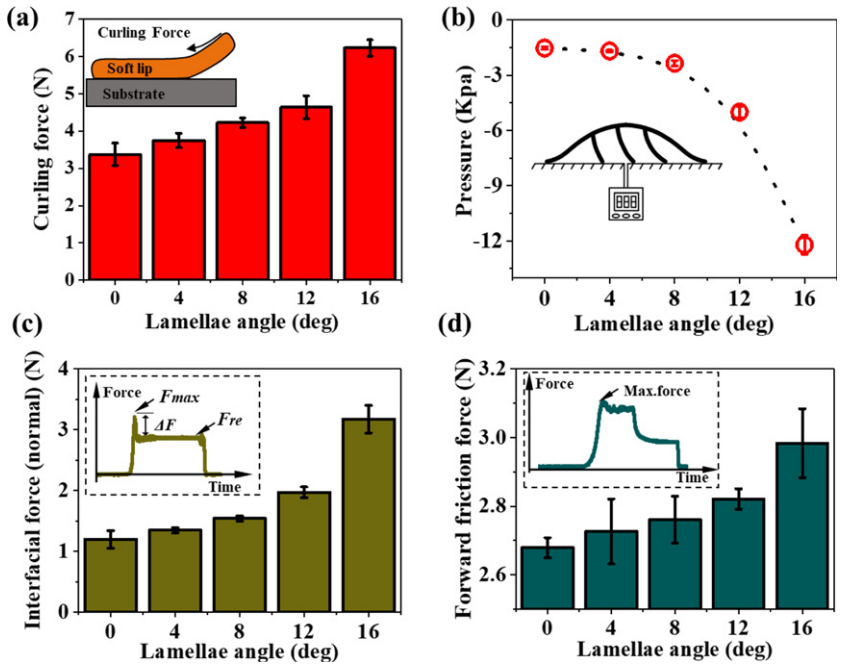

Figure 5. Effect of the lamellae motion on the adhesive performance during stage 1 of detachment. (a) Soft lip's curing force (F_c) as a function of the lamellae pitch angle (θ). (b) Chamber pressure differential of the disc prototype as a function of different lamellae pitch angle during the attached state. (c) Interfacial force ΔF (disc unsealed with the soft lip curling up) increased with the lamellae pitch angle. Inset panel: the vertical peeling force of the disc as a function of time on a smooth surface. The disc was pulled vertically up while fully immersed and unsealed with the soft lip curling. (d) Maximum forward frictional force as a function of the lamellae pitch angle. (Inset) frictional force as a function of time (lamellae pitch angle $\theta = 8°$).

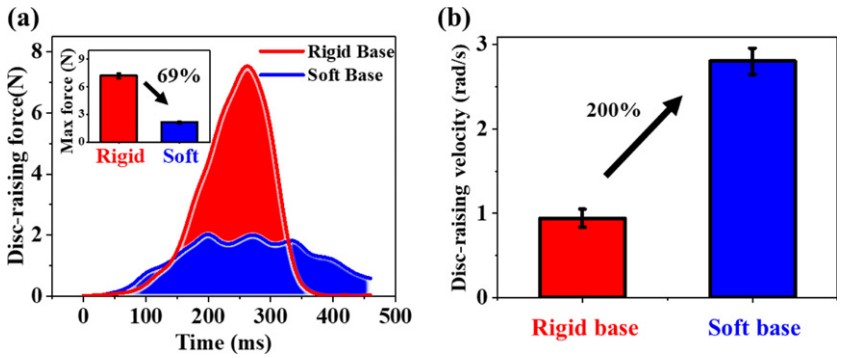

Figure 6. Detachment performance of the biomimetic remora disc during disc raising that mimics stage 2. (a) Disc-raising force required by the biomimetic suction disc with rigid or soft bases changes with time in the process of mimicking head raising (under the same disc raising velocity). (b) The angular velocity of the biomimetic suction discs with rigid vs soft bases in the process of mimicking stage 2 (under the same vertical pulling force).

Compared with the folded state (lamellae $\theta = 0°$), the interfacial force significantly increased by 166.4% when lamellae pitch angles increased from 4° to 16° (figure 5(c)).

According to previous studies [20, 28], remoras rotate their lamellae to press the spinules against the host surface to enhance the frictional force in the shear direction. Our kinematics videos showed that remoras commonly swim forward after detachment and we found that the forward frictional force of the robot was significantly decreased with a decreased lamellae angle (figure 5(d)). The maximum static frictional forces over a range of different lamellae pitch angles (from 0° to 16°) were acquired as shown in figure 5(d). The forward frictional force decreased significantly (11.2%, ANOVA, $F = 3.580$; d.f. $= 4$; $P < 0.05$), from 2.98 ± 0.10 to 2.68 ± 0.03 N when the lamellae fold from 16° to 0°. The inset shows the forward frictional force of the disc prototype (underwater, curling state, smooth surface) at $\theta = 8°$ versus time during a representative trial.

3.2.2. Detachment performance of stage 2

Figure 6 shows the detachment performance (force, speed and energy) of two biomimetic remora discs with soft versus rigid disc bases during the disc-raising process of stage 2 (Young's modulus of soft and rigid disc bases are 3 MPa and 3 GPa, respectively). From

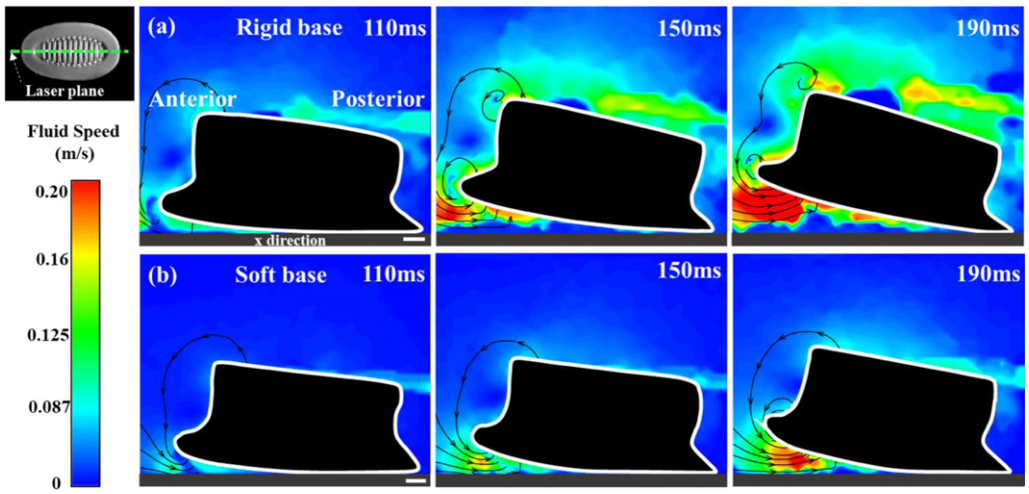

Figure 7. Hydrodynamic analysis of disc prototypes with both (a) rigid base and (b) soft base during the disc raising process that mimic stage 2, side views. Heat maps of fluid speed indicate the velocity in the *x*-direction of a downstream (red) moving fluid into the disc interior. The black arrow indicates the flow direction. The disc shape at each time is overlaid on each DPIV image. The laser plane is at the middle of the disc.

the force vs time curves in figure 6(a), we found that the forces to raise the two discs are significantly different (ANOVA, $F = 696.036$; d.f. $= 1$; $P < 0.05$) under the same pulling speed of 80 mm s^{-1}. The maximum force (inset panel) of the biomimetic disc with the rigid and soft base are 6.96 $\pm$ 0.48 N and 2.16 $\pm$ 0.12 N; while the energy consumption (force by vertical pulling distance) are 0.70 $\pm$ 0.08 J and 0.49 $\pm$ 0.014 J. Compared to the disc with a rigid base, the maximum force reduced by 69%, while the energy consumption reduced by 30%. Figure 6(b) shows the effect of the disc base stiffness on the disc's angular velocity under the same vertical pulling force (10 N). The results show that the angular velocity of the disc with the soft base increased from 0.94 $\pm$ 0.11 to 2.8 $\pm$ 0.16 rad s^{-1} (increased ~200%) compared with the velocity of the disc with a rigid base. This result indicates that the disc with a soft base detaches more rapidly than the disc with a rigid base when applying the same amount of force.

The hydrodynamics of biomimetic discs with soft and rigid bases during the disc-raising process was also investigated to understand the effect of the base stiffness on the detachment performance. We quantified fluid flow around the two prototypes at three different instants (110 ms, 150 ms and 190 ms) using digital particle image velocimetry (DPIV). The flow field of the suction discs with the rigid base and the soft base are shown in figures 7(a) and (b), respectively. As the suction discs gradually raised from the anterior, the external water rapidly flows into the interior of the disc. Comparing the flow field generated by the rigid-base disc and the soft-base disc, we found that the maximum water velocity (270 mm s^{-1}) generated by the disc with a rigid base is greater than that (200 mm s^{-1}) generated by the disc with a soft base. According to the fluid theory, increased water flow velocity would decrease the pressure at the disc-surface interface and increase the pressure differential between the upper- and lower-disc surfaces. This larger pressure differential may induce a greater drag force, slowing disc raising.

Images of the vortex generated by both soft-base and rigid-base discs are shown in figure 8. We observed that when the disc was lifted upward, an obvious leading-edge vortex (LEV) was formed underneath the anterior surfaces of both soft-base and rigid-base discs (figures 8(c) and (d)). We plotted vorticities of the LEV against the distance along the surface at three instants (150 ms, 190 ms and 230 ms) in figures 8(e)–(g). The distribution of the vorticity is a shift from a more Gaussian distribution of vorticity (at 150 ms) to a more bimodal distribution (at 230 ms), indicating a loss of coherence and separation of the LEV structure and the potential formation of a small additional vortex as the discs continue to rise. Along these transects, the vorticity strength gradually increased until it reaches a maximum, which reflects the vortex core of the LEV. At a position further away from the anterior part along the transects, the vorticity strength decreased to nearly zero. At 150 ms, 190 ms and 230 ms, we found that the maximum LEV vorticity of the rigid-base disc were 231%, 154% and 113% greater than those of the soft-base disc (see figures 8(e)–(g)). We provided schematic diagrams that show the disparity in strength and position of the leading-edge vortex (LEV) generated by the discs with the soft-base (figures 8(a)) and the rigid-base (figures 8(b)) during the raising process. From figures 8(a) and (b), at the same instance, the LEV (diameter of the vortex) of the rigid-base disc is stronger than that of the soft-base disc and the core of LEV generated by the rigid-base disc is closer to the anterior edge of the suction disc.

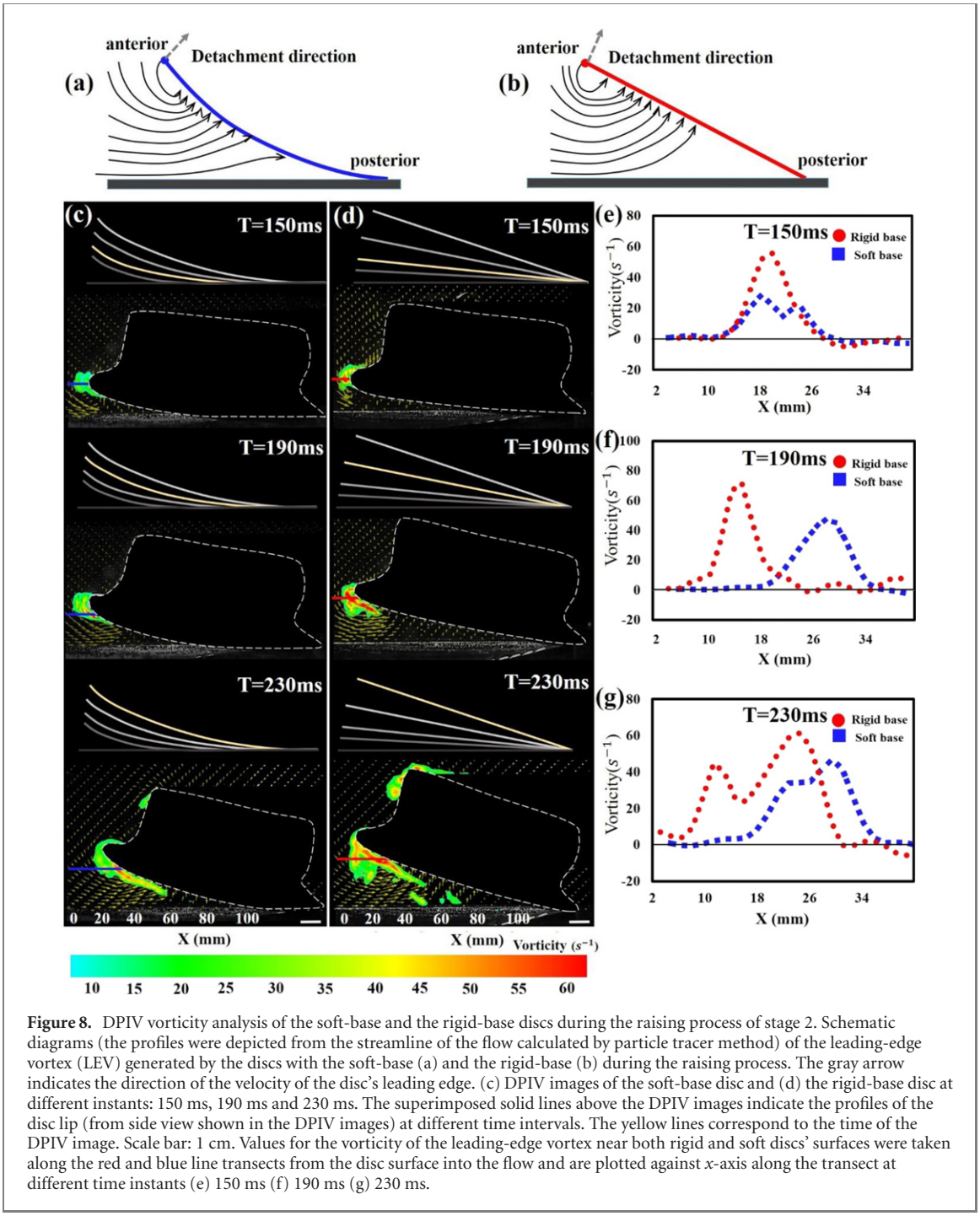

Figure 8. DPIV vorticity analysis of the soft-base and the rigid-base discs during the raising process of stage 2. Schematic diagrams (the profiles were depicted from the streamline of the flow calculated by particle tracer method) of the leading-edge vortex (LEV) generated by the discs with the soft-base (a) and the rigid-base (b) during the raising process. The gray arrow indicates the direction of the velocity of the disc's leading edge. (c) DPIV images of the soft-base disc and (d) the rigid-base disc at different instants: 150 ms, 190 ms and 230 ms. The superimposed solid lines above the DPIV images indicate the profiles of the disc lip (from side view shown in the DPIV images) at different time intervals. The yellow lines correspond to the time of the DPIV image. Scale bar: 1 cm. Values for the vorticity of the leading-edge vortex near both rigid and soft discs' surfaces were taken along the red and blue line transects from the disc surface into the flow and are plotted against *x*-axis along the transect at different time instants (e) 150 ms (f) 190 ms (g) 230 ms.

3.2.3. Detachment performance of stage 3

As previously mentioned, when the remora completely detached from a surface and started to swim, the adhesive disc profile reduces as the soft lip is adducted against the head and the lamellae fold down. We mimicked both flattened and erected states with the bio-robotic disc prototype (figure 9(a)) by programming the servo motors to switch between the attached and the detached state (movie S4). The thickness of the adhesive disc in the flattened state is 15.01 ± 0.48 mm (figure 9(b)) when the lamellae angle is 0 degree; while the thickness of the adhesive disc of the erected state is 12.45 ± 0.46 mm (figure 9(c)) when the lamellae angle is 16 degree. Then we investigated the fluid drag of both flattened and erected states using the disc prototype and 0.5 m s^{-1} flow and found that the average drag force of the disc is 314 ± 9.6 mN ($N = 5$) during the erected state; but only 175 ± 5.0 mN ($N = 5$) during the flattened state. Thus, the drag force was reduced 44% compared with the erected state (figure 9(d)).

3.3. Mimicking complete detachment using a simplified remora suckerfish robot

To demonstrate the entire detachment behavior of the biomimetic remora disc, we designed and fabricated a biomimetic remora robot with a rigid body (figures 10(a) and (b)). The robotic suckerfish is

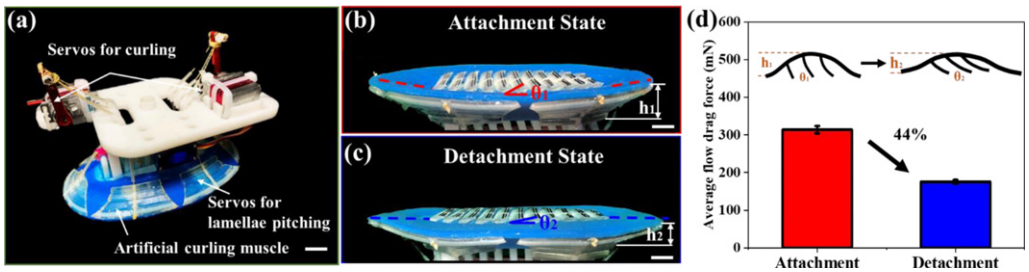

Figure 9. Detachment performance of the biomimetic remora disc during stage 3 (complete detachment state). (a) Photograph of the driving mechanism and the biomimetic suction disc. Six artificial curling muscles glued evenly around the soft lip. Through the cable-driven mechanism, two servos are used to curl the entire soft lip and one servo used to control the rotation of the lamellae. Scale bar 1 cm. (b) Attached state (soft lip is uncurled and lamellae erect) of the biomimetic suction disc. Scale bar 1 cm. (c) Detached state (soft lip is curled away from the surface and lamellae folded) of the biomimetic suction disc. Scale bar 1 cm. (b) and (c) are taken at the same camera angle. The movement of lamellae and soft lip results in different lamellae angles (θ) and thickness (h) of the suction disc. (d) The average flow drag force of the biomimetic suction disc under the condition of complete attachment and complete detachment. The flow direction is from anterior to posterior of the disc.

composed of four parts: a fish-like body, biomimetic suction disc, control unit and a jet propulsion component. The fish head and body are 3D printed individually with photosensitive resin and connected by hinges. The neck position of the robot fish has a wedge-shaped notch with an angle of approximately 30 degrees, which provides the flexibility of the neck needed for disc raising. Following the location of the biological suction disc, the first two-thirds of the suction disc is located on the head and the remaining one-third is fixed on the suckerfish body. The control system consists of a battery, a signal receiver and a servo. Three Kevlar ropes connect the artificial muscles on the suction disc to the servo and through this cable-driven design, the robotic fish can perform the curling and disc raising motion. For the jet propulsion unit, a pump draws water through a tube into the fish body and ejects water through the two outlets that are under the pectoral fins to provide thrust for detachment. Figure 10(c) demonstrates the complete detachment process of the robot remora in a water tank.

The robot exhibited similar detachment motions to its biological counterpart regarding mimicking stage 1–3 (movie S5). The entire detachment process of three stages took about 200 ms, which is even faster than the detachment of live remoras (240 ms) recorded in this study. The jet velocity of the water for propulsion at the outlets was 6.3 m s^{-1} and figure 10(d) shows the kinematics data (movement trajectory, x-direction speed, y-direction speed) of three independent detachment processes of the bionic remora robot. The experimental results show good repeatability of the robotic fish during the detachment process. The maximum speed in the x direction is 0.150 ± 0.006 m s^{-1} and the maximum speed in the y direction is 0.180 ± 0.004 m s^{-1}.

3.4. Application of the biomimetic suction disc

To demonstrate the applications of attachment and detachment performance of the biomimetic remora disc, we developed an underwater robot system that consists of a remotely operated vehicle (ROV) and two biomimetic remora discs attached on the top and bottom of the ROV with spring suspension (figure 11(a)). In this robotic system, the top disc was used to attach to overhanging surfaces, while the ventral disc was used to grasp objects. A hydraulic system was positioned inside of the ROV to control the detachment of both biomimetic suction discs (figure 11(b)). The schematic working principle is shown in figure 11(c). We demonstrated the performance of this robot through the transportation of objects in an underwater environment with intermediate stops (figure 11(d), supplementary movie S6). The entire process is as follows: (i) The ROV approached the object (∼1 kg) that needed to be transported. When it reached the top of the object, the bottom suction disc adhered to the object with the help of the preload generated by the downward thrust force from the vehicle's propellers. (ii) ROV carried the object to the overhanging surface (an acrylic plate) and attached to the surface using the top suction disc. (iii) The hydraulic system controlled the cable-driven mechanism of the top suction disc to detach from the overhanging surface. (iv) The ROV carried the object to the target location (a storage basket), the bottom suction disc detached and placed the object in the storage basket. This demonstration shows that the ROV has both hitchhiking and pick-and-place capabilities by integrating remora-inspired discs at appropriate locations.

4. Discussion

Compared with other fishes with adhesive organs, such as snailfishes [31], gobies [32] and clingfishes [33], remoras can achieve rapid, reversible adhesion on fast-moving hosts. Through the biological observation of live remoras, we separated the detachment process of remoras into three stages and conducted systematic tests on the effects of lamellae motion,

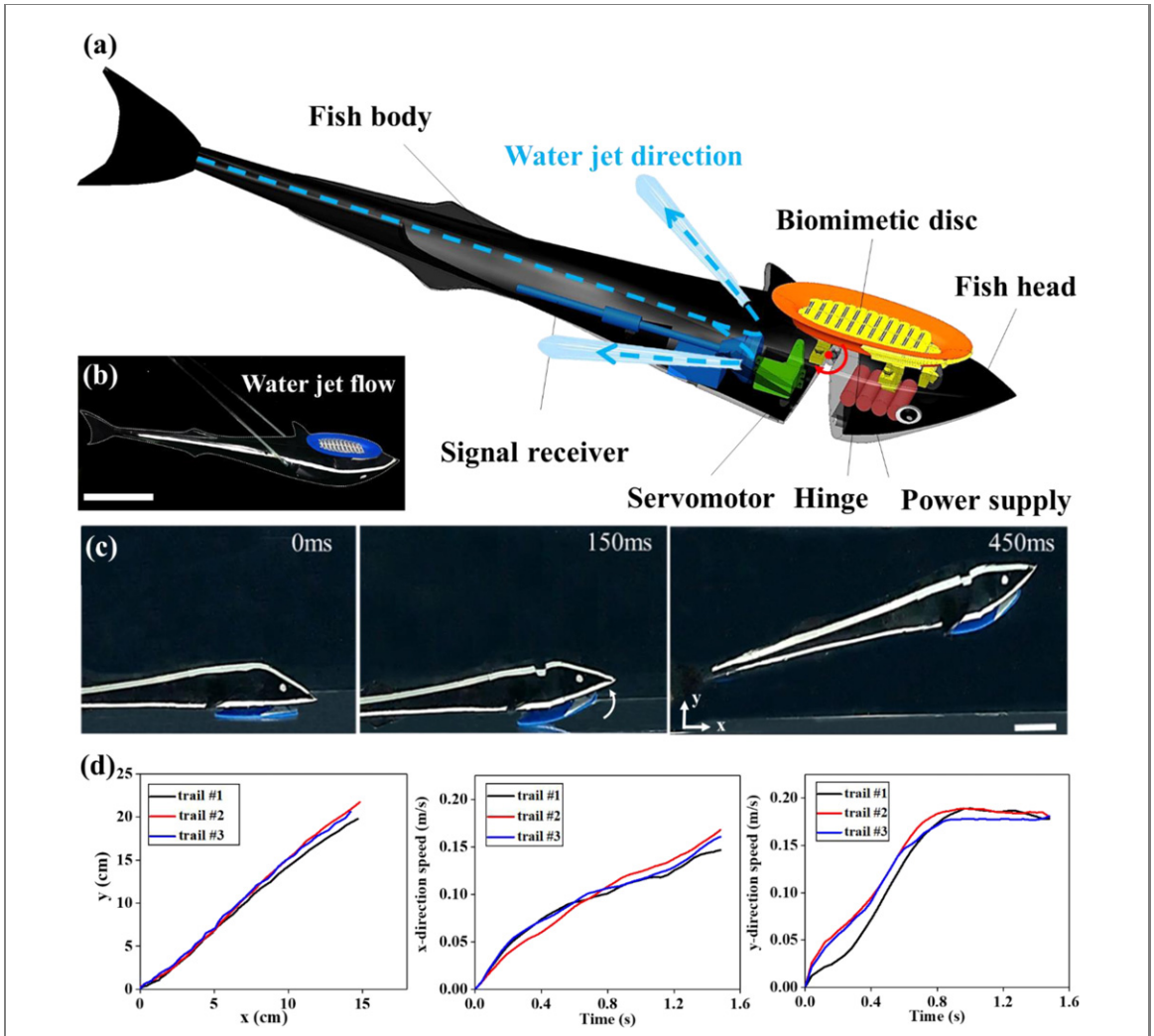

Figure 10. Bio-inspired remora suckerfish robot to demonstrate the detachment process. (a) Internal structure of the robotic fish that shows the detachment mechanism. (b) Photo of the robotic fish. Scale bar 10 cm. (c) Image sequence of when the robotic remora detaches from smooth substrates underwater and demonstrates stages 1–3. Scale bar 10 cm. The water jet speed is 6.3 m s^{-1}. (d) The kinematic data (*x*-axis velocity, *y*-axis velocity) of the robot's movement trajectory (tracking the neck position) during three detachment events.

disc flexibility, the disc lip motion on adhesive performance during detachment. Here we would like to discuss these effects, as well as the experimental results of the whole suckerfish robot.

Through high-speed videography, we find evidence indicating that remoras fold down their lamellae before the soft lip curls up, which can be viewed as the onset of the detachment process. Based on the experimental results of the biomimetic suction disc, we found erecting lamellae increased the inner volume of the suction disc and led to the increase of the pressure differential between the inner chamber and the external environment (figure 5(b)), which will increase the pressure acting on the soft lip. Additionally, as the lamellae pitch up, the contact area between the lamellae and the substrate increased, resulting in larger interfacial and friction force (figures 5(c) and (d)). Thus, we summarized that the folding down of lamellae during the detachment process primarily played two roles: (1) significantly reducing the force of curling the soft lip for releasing the seal (up to ∼50%); (2) weakening the interlock and contact area between the lamellae (including both lamellae soft tissue and spinules) and the substrate. For example, compared with fully erected lamellae (16°), the vertical interfacial force and the forward frictional force with folded lamellae (0°) decreased by 62% and 10%, respectively. After the lamellae folded down, the curling of the soft lip propagated from anterior to posterior to rapidly break the suction seal. Curling the soft lip only required 3.3 N, which is 94 times smaller than the vertical pull-off force (311.8 N) to break the seal.

The biological suction disc of a remora is flexible and we found that the adhesive disc bent during head raising in stage 2. The robotic experiments showed that the soft base of the disc pad played an essential role in detachment performance. In particular, we found the suction disc with a soft base requires less force to be peeled away from the surface than that of a disc with a rigid base when peeled at the same speed. When imposing the same pulling force, the peeling velocity of the disc with the soft-base is also notably

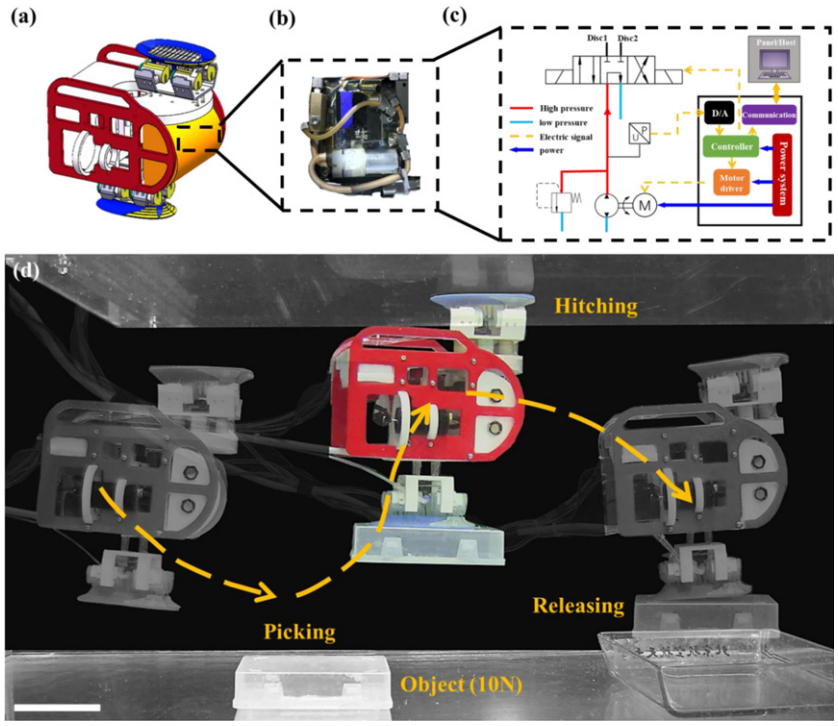

Figure 11. Extended application of the biomimetic suction disc underwater. (a) An integrated underwater vehicle, which consists of an ROV, two biomimetic suction discs and (b) and (c) a custom hydraulic system. (d) Demonstrates a potential underwater application scenario of the ROV. Scale bar, 10 cm.

faster due to the flexibility. The stiffness of the disc may also have an impact on the leading-edge vortex, which would, in turn, affect the fluid resistance force generated by the disc. We show that the rigid-base disc generated a stronger LEV than the soft-base disc, which had peak vorticity 231% more than the soft-base disc (at 150 ms). A more systematic study on the hydrodynamics of the hitchhiking behavior will be conducted in the future.

Accordingly to our observations, the entire suction disc kept a flattened profile (with lip adducted against the head and lamellae folded down) when remoras completed detachment and started to swim. We show that the flow drag force was reduced by 44% from the flattened state to the erected state used during attachment. This result indicates that the remora's disc can morph to minimize fluid drag during free-swimming behaviors.

Stage 3 involves both detachment of the adhesive disc and the undulatory body and fins. In this study, we demonstrated the entire detachment mechanism of the remora disc through a bio-inspired remora robot. The current robotic fish's body is rigid and does not incorporate movement of the body and fins, but instead it used a simplified approach—using two jets at the pectoral fin positions to locomote away from surfaces. Future research work will include observations of the entire body and fins of remora, as well as exploring the mechanism of biological adhesion through a fully untethered biomimetic robotic suckerfish with a compact adhesive disc.

We demonstrated the potential application prospects of the biomimetic suction disc by implementing two discs on an underwater ROV. Through the use of two biomimetic suction discs, the ROV possesses the capabilities of both 'hitching' and 'pick and place'. This scalable ability of the biomimetic suction disc endows the current ROV with broad applications including long-term underwater transportation, archeology, search and rescue, and biological observation.

In our previous study [28], we achieved detachment of the biomimetic suction disc by pumping water into the disc cavity, which is a common approach for detaching suction cups in industrial applications. For robotic applications, water injection requires a set of supporting devices, such as a pump, hydraulic motor, solenoid valve and control system, which altogether has a large mass, bulky volume and high-power consumption. In addition, sealing all these components for underwater use is a challenge. In contrast, the lip-curling approach for detachment is biomimetic and benefits from comparative simplicity. As shown in figure 9(a), the system of the biomimetic detachment mechanism is very simple- just a small servo motor (∼20 g) and a lightweight cable mechanism (a few grams). The small volume of the motor and mechanism makes it easy to miniaturize and integrate into an underwater robot. Since the force required to achieve detachment by curling the soft lip is small (less than 3 N) and the necessary components are easier to incorporate,

we believe the biomimetic lip-curling approach represents a substantial improvement compared to water pumping.

5. Conclusions

In this work, we investigated the detachment mechanism of the remora's suction disc. We found that the detachment of live remoras' disc can be separated into three stages: (i) lamellae folding down and soft lip curling, (ii) disc raising and (iii) complete detachment and disc flattening. We fabricated a biomimetic remora disc prototype to assist in investigating each stage of the detachment mechanism. We found that the functional structures (disc lip, lamellae, spinules and disc base) of the remora suction disc and the coordinated motion of these structures achieves efficient detachment (faster and less energy consumption). We mimicked the entire detachment using a simplified remora suckerfish robot which uses water jets as a propelling source. We demonstrated the potential future applications of the biomimetic suction disc by using an underwater ROV. Our study lays a foundation for understanding the detachment process of a suckerfish and may inspire future reversible underwater bio-inspired adhesion devices.

Acknowledgments

This work was supported by the National Science Foundation support projects, China (Grant No. 91848105), in part by National Key R & D Program of China (Grant No. 18YFB1304600), and National Science Foundation support projects 61822303, 61633004, 91848206. Permission of reusing the material from the previous work of our group (Wang *et al*, 2019) is authorized by IEEE. We thank Andy Williston and Meaghan Sorce at the Museum of Comparative Zoology for help accessing the ichthyological collections.

ORCID iDs

Li Wen https://orcid.org/0000-0002-1498-3103

References

[1] Chan T S and Carlson A 2019 Physics of adhesive organs in animals *Eur. Phys. J.: Spec. Top.* **227** 2501–12
[2] Labonte D and Federle W 2015 Scaling and biomechanics of surface attachment in climbing animals *Phil. Trans. R. Soc.* B **370** 20140027
[3] Federle W, Riehle M, Curtis A S and Full R J 2002 An integrative study of insect adhesion: mechanics and wet adhesion of pretarsal pads in ants *Integr. Comp. Biol.* **42** 1100–6
[4] Dai Z, Gorb S N and Schwarz U 2002 Roughness-dependent friction force of the tarsal claw system in the beetle *Pachnoda marginata* (Coleoptera, Scarabaeidae) *J. Exp. Biol.* **205** 2479–88
[5] Niederegger S and Gorb S 2003 Tarsal movements in flies during leg attachment and detachment on a smooth substrate *J. Insect Physiol.* **49** 611–20
[6] Clemente C J and Federle W 2008 Pushing versus pulling: division of labour between tarsal attachment pads in cockroaches *Phil. Trans. R. Soc. B.* **275** 1329–36
[7] Tian Y, Pesika N, Zeng H, Rosenberg K, Zhao B, McGuiggan P, Autumn K and Israelachvili J 2006 Adhesion and friction in gecko toe attachment and detachment *Proc. Natl Acad. Sci. USA* **103** 19320–5
[8] Hanna G, Jon W and Barnes W P J O N 1991 Adhesion and detachment of the toe pads of tree frogs *J. Exp. Biol.* **155** 103–25
[9] Lee H, Lee B P and Messersmith P B 2007 A reversible wet/dry adhesive inspired by mussels and geckos *Nature* **448** 338
[10] Cha H J, Hwang D S and Lim S 2008 Development of bioadhesives from marine mussels *Biotechnol.* J **3** 631–8
[11] Sundaram S, Josekutty C J and Chavan B B 2011 Length-weight relationship of green mussel *Perna viridis* (Linnaeus, 1758) from Versova Creek, Mumba *Mar. Fish. Inf. Serv.* **207** 34
[12] Nesis K N 1987 *Cephalopods of the World: Squids, Cuttlefishes, Octopuses, and Allies* (Neptune City, NJ: TFH Publications)
[13] Ditsche P and Summers A 2019 Learning from Northern clingfish (*Gobiesox maeandricus*): bioinspired suction cups attach to rough surfaces *Phil. Trans. R. Soc.* B **374** 20190204
[14] Wainwright D K, Kleinteich T, Kleinteich A, Gorb S N and Summers A P 2013 Stick tight: suction adhesion on irregular surfaces in the northern clingfish *Biol. Lett.* **9** 20130234
[15] Sandoval J A, Jadhav S, Quan H, Deheyn D D and Tolley M T 2019 Reversible adhesion to rough surfaces both in and out of water, inspired by the clingfish suction disc *Bioinspiration Biomimetics* **14** 066016
[16] Strasburg W 1964 Further notes on the identification and biology of echeneid fishes *Pac. Sci.* **18** 51–7
[17] Sazima I and Grossman A 2006 Turtle riders: remoras on marine turtles in Southwest Atlantic *Neotrop. Ichthyol.* **4** 123–6
[18] Fulcher B A and Motta P J 2006 Suction disk performance of echeneid fishes *Can. J. Zool.* **84** 42–50
[19] Nadler J H, Mercer A J, Culler M, Ledford K A, Bloomquist R and Lin A 2013 Structures and function of remora adhesion *MRS Online Proc. Libr.* **1498** 159–68
[20] Beckert M, Flammang B E and Nadler J H 2015 Remora fish suction pad attachment is enhanced by spinule friction *J. Exp. Biol.* **218** 3551–8
[21] Beckert M, Flammang B E, Anderson E J and Nadler J H 2016 Theoretical and computational fluid dynamics of an attached remora (*Echeneis naucrates*) *Zoology* **119** 430–8
[22] Cohen K E, Flammang B E, Crawford C H and Hernandez L P 2020 Knowing when to stick: touch receptors found in the remora adhesive disc *R. Soc. Open Sci.* **7** 190990
[23] Lee S H, Song H W, Kang B S and Kwak M K 2019 Remora-inspired reversible adhesive for underwater applications *ACS Appl. Mater. Interfaces* **11** 47571–6
[24] Gamel K M, Garner A M and Flammang B E 2019 Bioinspired remora adhesive disc offers insight into evolution *Bioinspiration Biomimetics* **14** 056014
[25] Gu Z, Li S, Zhang F and Wang S 2016 Understanding surface adhesion in nature: a peeling model *Adv. Sci.* **3** 1500327
[26] Meitl M A, Zhu Z T, Kumar V, Lee K J, Feng X, Huang Y Y, Adesida I, Nuzzo R G and Rogers J A 2006 Transfer printing by kinetic control of adhesion to an elastomeric stamp *Nat. Mater.* **5** 33
[27] Yang S Y *et al* 2012 Elastomer surfaces with directionally dependent adhesion strength and their use in transfer printing with continuous roll-to-roll applications *Adv.Mater.* **24** 2117–22
[28] Wang Y *et al* 2017 A biorobotic adhesive disc for underwater hitchhiking inspired by the remora suckerfish *Sci. Robot.* **2** eaan8072
[29] Wang S *et al* 2019 A bio-robotic remora disc with attachment and detachment capabilities for reversible

underwater hitchhiking *IEEE Int. Conf. Rob. Autom.* pp 4653–9
[30] Su S *et al* 2020 Vertical fibrous morphology and structure-function relationship in natural and biomimetic suction-based adhesion discs *Matter* **2** 1207–21
[31] Budney L A and Hall B K 2010 Comparative morphology and osteology of pelvic fin-derived midline suckers in lumpfishes, snailfishes and gobies *J. Appl. Ichthyol.* **26** 167–75
[32] Maie T, Schoenfuss H L and Blob R W 2012 Performance and scaling of a novel locomotor structure: adhesive capacity of climbing gobiid fishes *J. Exp. Biol.* **215** 3925–36
[33] Ditsche P, Wainwright D K and Summers A P 2014 Attachment to challenging substrates—fouling, roughness and limits of adhesion in the northern clingfish (*Gobiesox maeandricus*) *J. Exp. Biol.* **217** 2548–54